Accepted Manuscript

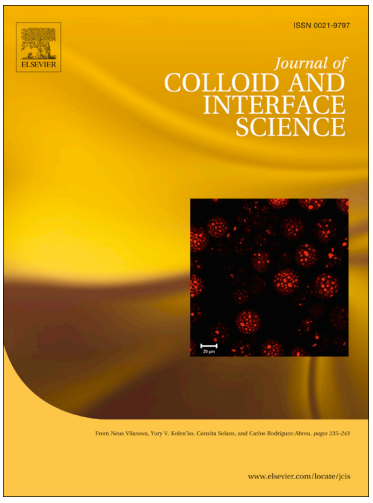

Au@CdSe heteroepitaxial nanorods: an example of metal nanorods fully covered by a semiconductor shell with strong photo-induced interfacial charge transfer effects

Suh-Ciuan Lim, Wen-Fu Lo, Po-Yuan Yang, Shu-Chen Lu, Anneli Joplin, Stephan Link, Wei-Shun Chang, Hsing-Yu Tuan

PII: S0021-9797(18)30836-1
DOI: https://doi.org/10.1016/j.jcis.2018.07.080
Reference: YJCIS 23871

To appear in: *Journal of Colloid and Interface Science*

Received Date: 10 May 2018
Revised Date: 14 July 2018
Accepted Date: 20 July 2018

Please cite this article as: S-C. Lim, W-F. Lo, P-Y. Yang, S-C. Lu, A. Joplin, S. Link, W-S. Chang, H-Y. Tuan, Au@CdSe heteroepitaxial nanorods: an example of metal nanorods fully covered by a semiconductor shell with strong photo-induced interfacial charge transfer effects, *Journal of Colloid and Interface Science* (2018), doi: https://doi.org/10.1016/j.jcis.2018.07.080

Au@CdSe heteroepitaxial nanorods: an example of metal nanorods fully covered by a semiconductor shell with strong photo-induced interfacial charge transfer effects

Suh-Ciuan Lim[a], *Wen-Fu Lo*[a], *Po-Yuan Yang*[a], *Shu-Chen Lu*[a], *Anneli Joplin*[b], *Stephan Link*[b], *Wei-Shun Chang*[b, c*] *and Hsing-Yu Tuan*[a]*

[a]Department of Chemical Engineering, National Tsing Hua University, 101, Section 2, Kuang-Fu Road, Hsinchu, Taiwan 30013, ROC.

[b]Department of Chemistry, Rice University, 6100 Main Street, Houston, Texas 77005, United States

[c]President address:Department of Chemistry and Biochemistry, University of Massachusetts Dartmouth, 285 Old Westport Rd, North Dartmouth, Massachusetts 02747, United States

*Corresponding author

Email address: wchang2@umassd.edu

Email address: hytuan@che.nthu.edu.tw

Abstract

Synthesis of metal@semiconductor heteroepitaxial nanorods fully covered by a semiconductor shell remains challenging due to the large lattice mismatch between the two components. Here, we prepared Au@CdSe heteroepitaxial nanorods by employing pre-growth of Ag_2Se as an intermediate layer that favored the formation of a complete CdSe shell via a cation-exchange process. The optical properties of these hybrid nanostructures can be tailored by changing the shell thickness with thicker shells resulting in a redshift of the longitudinal surface plasmon resonance (SPR). The resonance energy, intensity and linewidth of the longitudinal surface plasmon resonance were measured by single-particle dark-field scattering (DFS) spectroscopy, confirming significant electron transfer from the Au nanorod to the CdSe shell. In addition, we also studied the dependence of the catalytic reacitivty on shell thickness in photocatalysis of methylene blue under UV illumination. These studies revealed that a thinner shell thickness resulted in higher photocatalytic activity.

***Keywords**:* metal@semiconductor, heteroepitaxial nanorods, cation-exchange process, surface plasmon resonance, single-particle dark-field scattering, photocatalytic activity

1. Introduction

Noble metal nanomaterials have attracted much research attention in the physical, chemical, and material sciences because of their surface plasmon resonance (SPR)[1-4]. The optical properties of the SPR are very sensitive to the shape, size and constituent materials of the nanostructures as well as their surrounding medium. There are several approaches to manipulate the energy and lineshape of the SPR spectra. For example, by changing the nanoparticle shape from spheres to rods, the SPR spectra split into transverse and longitudinal modes with an SPR parallel to the short and long axes of the nanorods, respectively. Covering metallic nanostructures with another material to create heterostructures is an alternative way to dramatically tune their optical properties. The latter method includes two general approaches. The first approach is to form a metallic shell outside of the metal nanoparticle creating a metal@metal nanostructure such as Au@Ag [5-7]. The SPR bands of Au@Ag core-shell structures are blueshifted compared to Au nanostructures due to the different dielectric constant of the shell, which supports a SPR. The other approach is to form hybrid nanostructures from two different types of materials. For example, metal@magnet[8-11], metal@semiconductor[12-15] and semiconductor@semiconductor[16, 17] hybrid structures have already been demonstrated with Au@TiO_2 core-shell structures[18-20] being the most frequently reported in the literature. In the case of Au@TiO_2 nanostructures the effective refractive index around Au increases inducing a redshift of the SPR with increasing TiO_2 shell thickness. Additionally, other researchers have shown modulation of the SPR in Au nanostructures by forming metal@chalcogenide core-shell structures [21-23].

Among potential hybrid nanostructures, metal@semiconductor core-shell heterostructures have been extensively studied because this type of composite combines two disparate materials

to form a unique structure with synergetic properties and functionalities. For example, in metal@semiconductor heterostructures, the metal domains may serve as anchoring sites for assembly of various structures[24]. Additionally, the metallic components can greatly increase the light absorption efficiency[25, 26] and the photocatalytic reactivity of semiconductors by improving charge separation[27-29]. Moreover, metallic components can also modify the nonlinear optical properties and change the photoluminescence (PL) behavior of semiconductors[30, 31]. The developments in metal@semiconductor synthesis included a wide variety of methods, fabrication of metal@semiconductor heteroepitaxial nanostructures with complete semiconductor shells has been regarded as tremendous challenge because of the large lattice mismatch between these components and has been demonstrated in recent studies[32-34]. Many efforts have been devoted to the synthesis of this type of heterostructure including the selective deposition of metals onto semiconductor tips[35-39], the diffusion of metal seeds into semiconductor solutions, and growth of semiconductors on metal seeds[26],[40-42]. Furthermore, the synthesis of metal-semiconductor core-shell heterostructures is of particular interest because these heterostructures can maximize the interfacial area between components and thus provide an outstanding platform for achieving charge separation and exciton-plasmon interactions. Wang et al. used $Cu(NO_3)_2$ as precursor to form a Cu_2O shell on Au spheres[12]. Talapin et al. prepared Au@PbS core-shell heterostructures in the oil phase using PbS-oleate as precursor[13]. Wang et al. further synthesized different Au@sulfide heterostructures by binding metal thiobenzoates onto various Au structures[26]. These strategies all relied on particular metal precursors for the growth of heterostructures. Among methods for the synthesis of metal@semiconductor core-shell heterostructures, the cation-exchange reaction stands out. This technology was established by Alivisatos et al. and provides a brand-new strategy for transformation of materials from one crystalline solid to

another[43, 44]. In a cation-exchange process, the composition of the material is altered by replacing one cation with another substitutional metal ion. For example, CdSe is transformed into Ag_2Se by adding a solution containing Ag^+ cations into a suspension of CdSe nanocrystals, and the reverse reaction from Ag_2Se to CdSe is favored upon addition of Cd^{2+}[45]. However, the transform from Ag_2Se to CdSe is thermodynamically unfavorable. It can only happen when a complex ligand such as TBP or TOP is employed[46, 47]. Remarkably, the morphology of the nanocrystals remains unchanged after the cation-exchange process.

UV-visible light photocatalysis can effectively convert solar energy to chemical energy. In the past few years, extensive effort has been devoted to the study of semiconductor photocatalysts because of their ability to convert photon energy into chemical energy. The key step in photocatalysis is effective charge separation of electron-hole pairs. Single component semiconductor nanomaterials display relatively poor photocatalytic efficiency because the light-induced charge carriers easily diffuse back into the semiconductor domain and undergo recombination. However, metal@semiconductor hybrid structures can enhance charge separation to suppress the recombination of photogenerated electrons and holes, and thus have been extensively used in photocatalysis[41, 48-52]. The most common semiconductor components applied are metal oxides like ZnO[45,53, 54] or TiO_2[46-48]. For example, Li et al. successfully synthesized Au@ZnO hybrid nanoparticles to catalyze the reaction of rhodamine B (RhB) dye molecules[45]. Additionally, Kamat et al. prepared Au-capped TiO_2 nanoparticles which were used to generate thiocyanate ions (SCN^-) at the semiconductor interface[55]. However, one disadvantage of these systems is that light absorption is limited in metal oxides to a smaller spectral region because of their larger bandgap energies. CdSe is another promising material for photocatalysis because its smaller bandgap energy of 1.7 eV allows for broad size-dependent spectral tuning within the visible light spectral range. Charge separation in CdSe nanocrystals was previously reported

when they were combined with semiconducting polymers or organometallic compounds[56-59]. For example, Banin et al. demonstrated light-induced generation of electron-hole pairs in CdSe@Au nanodumbells (NDBs), which were also effective in the photocatalytic reduction of methylene blue molecules[34]. Furthermore, additional research using CdSe@Pt nanoparticles proved that photocatalysis is dependent on the morphology of the hybrid structures[24].

In this research, we established a strategy for obtaining Au@CdSe core-shell heterostructures by pre-growth of Au nanorods as structure-directing cores for further synthesis. This method relied on the pre-growth of Ag_2Se as an intermediate layer that favored the formation of a CdSe shell in a subsequent cation-exchange reaction. We controlled shell thickness via the amount of Cd^{2+} ions in the solution based on the relative concentration. The photocatalytic properties of these hybrid structures were investigated via reduction of methylene blue (MB) under UV irradiation at 254 nm to reveal the relationship between the photocatalytic reactivity and the shell thickness.

2. Experimental

2.1 Chemicals

All chemicals were used as received without additional purification. Gold chloride trihydrate ($HAuCl_4 \cdot 3H_2O$, 99.9%), sodium borohydride ($NaBH_4$, 99%), silver nitrate ($AgNO_3$, 99%), L-ascorbic acid (99%), hexadecyltrimethylammonium bromide (CTAB, 99%), polyvinylpyrrolidone, cadmium nitride tetrahydrate ($Cd(NO_3)_2$, 99.999%), sodium hydrate (NaOH, 99.998%), and methylene blue were all purchased from Sigma-Aldrich. Selenourea (99%) was purchased from Alfa Aesar.

2.2 Synthesis of Au nanorods

The Au nanorods were prepared in aqueous solution using a seed-mediated growth method. First, the Au seed solution was prepared by adding 0.25 mL of 0.01 M $HAuCl_4$ solution into 9.75 mL of 0.01 M CTAB. A freshly prepared 0.6 mL solution of 0.01 M $NaBH_4$ was injected drop-by-drop into that mixture and the solution was vigorously stirred for 2 hours. Next, the growth solution was prepared by combining 0.95 mL of 0.01 M $AgNO_3$, 5 mL of 0.01 M $HAuCl_4$, and 9.5 mL of 0.01 M CTAB followed by the addition of 0.55 mL of 0.1 M ascorbic acid. The solution became colorless after the addition of ascorbic acid. Finally, 0.12 mL of seed solution was injected into the growth solution and stirred for 12 hours. The product was centrifuged at 8000 rpm for 5 min several times and the collected precipitate was dispersed in 10 mL of DI water.

2.3 Synthesis of Au@CdSe Core-Shell Heterostructures

The three steps to obtain Au@Ag, Au@Ag_2Se and Au@CdSe nanorods are as follows:

Step 1: For the Au@Ag nanorod synthesis, 0.8 mL of the prepared Au nanorod solution was mixed with 0.1 M CTAB and 3.2 mL of 1 wt% PVP solution. Next, 1 mM $AgNO_3$, 0.1 M ascorbic acid and 0.2 M NaOH solution were added to the mixture solution to maintain a volumetric ratio of mixture solution, ascorbic acid and NaOH as 60:25:50. After NaOH was injected, the color of the solution changed rapidly indicating formation of the Ag shell.

Step 2: The as-prepared Au@Ag nanorods were dispersed in 3 mL of DI water. Au@Ag_2Se nanorods were obtained by mixing an excess of selenourea solution with the Au@Ag nanorod solution. The Ag_2Se shell was formed after stirring for 30 minutes. The Au@Ag_2Se nanorods were used as prepared to grow Au@CdSe nanorods.

Step 3: 0.1 M $Cd(NO_3)_2$ solution was prepared and injected in different amounts (Table S1) into the Au@Ag_2Se nanorod solution. The solution was kept at 50 ˚C and stirred for 60 minutes. The final product was centrifuged and the collected precipitate was dispersed in DI water.

2.4 Photocatalysis of Au@CdSe hybrid structures

Different shell thicknesses of 1 mg Au@CdSe nanorods dispersed in 1 ml DI water were prepared and added to 10 mL of 10^{-5} M methylene blue (MB) aqueous solution. The solutions were stirred in a dark room until an adsorption equilibrium was reached. Subsequently, the solutions were exposed to UV radiation using a 4 W/115 V- 60 Hz/ 0.16 Amps UV lamp in different time intervals. After exposure, the samples were centrifuged to remove the Au@CdSe photocatalysts. The change in MB absorption was measured using a UV-visible spectrophotometer to determine the concentration of MB. The degradation efficiency of the MB can be defined as follows[60]:

Degradation (P%) = $(1-C/C_0) \times 100\%$

where C_0 is the initial concentration of MB at adsorption equilibrium, and C is the residual concentration of MB at each time interval.

2.5 Characterization

Transmission electron microscopy (TEM) was performed using a Hitachi H-7100 electron microscope with an accelerating voltage of 75kV. High-resolution TEM (HRTEM), selected area diffraction (SAED) and EDX analysis were obtained using a JEOL JEM 2100F electron microscope with an accelerating voltage of 200 kV. UV-visible spectra were characterized using a Hitachi U-4100 spectrophotometer under atmospheric conditions.

Single-particle dark-field scattering (DFS) spectra were acquired using a home-built microscope based on a commercial microscope (Zeiss, Observer 1m) with a transmission dark-field geometry. Unpolarized light from a halogen lamp (100W) was focused on the sample through an oil-immersion dark-field condenser (N.A. =1.4) and the scattered light from single nanoparticles was collected via an air-space objective (N.A. =0.8). The image was focused onto a 50 μm pin hole and then directed to a spectrometer (Princeton Instruments, SP2150) equipped with a CCD camera (Princeton Instruments, BR400). The pinhole replicated a confocal scheme and only transmitted the scattered light from a specific region of interest. All single-particle spectra were corrected for the background scattering of the substrate and normalized by the lamp spectrum. The data were analyzed using a home-made Matlab script. The nanoparticles were deposited on a quartz substrate with a microscale Au pattern to allow identification of the same nanoparticles in optical and electron microscopes.

3. Results and discussion

The synthesis scheme is displayed in Scheme 1, and each stage is characterized by TEM images as shown in Fig. 1. Fig. 1a shows that the longitudinal axis and transverse axis of the Au nanorods were 20-36 nm and 8-16 nm, respectively. Sodium citrate was used as a surfactant for formation of the Ag shell in previous reports[6]. However, due to relatively low reproducibility, we used polyvinyloyrrolindone (PVP) and cetyltrimethyl ammonium (CTAB) as our surfactants instead of sodium citrate. Fig. 1b shows a TEM image of the Au@Ag core-shell structures. A homogeneous Ag layer is easily deposited on the surface of the Au nanorods because of the perfect lattice match between these two metals. However, the similar lattice spacing makes it difficult to identify the interfacial area of Au@Ag and hard to measure the Ag shell thickness quantitatively[6]. In order to obtain Au@CdSe core-shell heterostructures, we formed an

intermediate layer of Ag_2Se, which favors CdSe shell formation via a cation-exchange reaction. It is very important for this process to occur under an oxygen rich environment based on the balanced reaction, which is shown below:

$$4\ Ag + 2\ Se^{2-} + O_2 + 2\ H_2O \rightarrow 2\ Ag_2Se + 4\ OH^-$$

Fig. 1c shows TEM images of $Au@Ag_2Se$ core-shell heterostructures and the shell thickness of Ag_2Se is almost the same as the Ag layer. The cation-exchange process represents a general approach for preparing various metal-chalcogenide heterostructures in previous reports[26,40,[61]]. In this research, the intermediate Ag_2Se shell was transformed into a CdSe shell by adding a certain amount of aqueous $Cd(NO_3)_2$ to the $Au@Ag_2Se$ solution. The excess Cd^{2+} ions reacted with residual selenide in the solution promoting CdSe shell growth. The final Au@CdSe core-shell heterostructures exhibited a shell thickness of 3.6 nm as shown in Fig. 1d. Furthermore, the thickness of the CdSe shell can be modulated by adding different amounts of aqueous $Cd(NO_3)_2$ to the $Au@Ag_2Se$ solution. The $Cd(NO_3)_2$ concentrations are 9.8, 10, 12.4, 12.9 mM for the formation of 2-3, 4-6, 6-8, 9-11 nm CdSe shell thickness, respectively. The composition of the shell on the Au nanorods was indicated by the color of the solution and the SPR wavelengths of the hybrid structures as shown in Fig. 2. The original longitudinal SPR (LSPR) of the bare Au nanorods was centered at about 800 nm, and the transverse SPR (TSPR) band appeared at around 520 nm. The LSPR wavelength of Au@Ag nanorods blueshifted to 735 nm after Ag coating, and the color of the solution changed from pink to green. After the Ag layer was converted to an Ag_2Se layer, the LSPR wavelength redshifted to 900 nm due to the higher refractive index of Ag_2Se[62], and the solution color changed from green to purple-red. Finally, the LSPR wavelength of the Au@CdSe hybrid structure further

redshifted to about 960 nm after the cation-exchange reaction while the corresponding solution color changed from purple-red to gray. In contrast to the LSPR, the TSPR wavelength at each stage barely shifted.

Fig. 3 illustrates the detailed crystallographic geometry and composition of the intermediate Au@Ag_2Se core-shell nanorods. Fig. 3a shows the high-resolution TEM (HRTEM) image of a single nanorod and the inset is a fast Fourier transform (FFT) of the square region, indicating the (121) crystal plane of the Ag_2Se shell. A HRTEM image was also obtained for the interface of the core and the shell region as shown in Fig. 3b. The parallel lattice planes for the Au-core and Ag_2Se-shell were 0.236 nm and 0.258 nm, in agreement with the (111) lattice plane of a face-centered cubic Au crystal and the (121) lattice plane of an orthorhombic structure of Ag_2Se, respectively. Fig. 3c shows a typical selected area electron diffraction (SAED) pattern of the sample shown in Fig. 3a. The diffraction pattern indicates the polycrystallinity of the Ag_2Se shell with an orthorhombic structure. To further confirm the composition of the samples, we investigated them by energy dispersive x-ray spectroscopy (EDS) analysis as shown in Fig. 3d. The EDS spectrum shows Au, Ag and Se peaks in addition to the C, O and Cu peaks generated by the carbon-coated copper grid. Fig. 4 presents the detailed crystallographic geometry and composition of the Au@CdSe core-shell nanorods. To confirm the heteroepitaxial growth of the core-shell hybrid structure, the final products were analyzed by high-resolution TEM and SAED. Fig. 4a displays a HRTEM image of a single Au@CdSe nanorod and the inset is a FFT of the square region, indicating the (102) crystal plane of the CdSe shell. A HRTEM image was also acquired at the interface of the Au-core and the CdSe-shell and is shown in Fig. 4b. Two distinct sets of lattice fringes can be clearly observed. In the

core region, an interlayer spacing of 0.202 nm is obtained, which corresponds to the d-spacing of the (200) crystal plane of the fcc Au. In the shell region, an interlayer spacing of 0.255 nm was obtained, which agrees with the d-spacing of the (102) crystal plane of the wurtzite structure of CdSe and it is found to grow heteroepitaxially on the (200) plane of Au. The SAED pattern recorded on the CdSe shell in Fig. 4c demonstrates that the structure of the final product was polycrystalline and consisted of the wurtzite phase of CdSe. In order to confirm the composition of the final products, we characterized them by EDS as shown in Fig. 4d. The EDS spectrum exhibits Au, Se and Cd signals as well as the C, O and Cu peaks attributed to the carbon-coated copper grid. Additionally, to more clearly reveal the spatial distribution of Au, Cd and Se within the heterostructures, we performed high-angle annular dark-field scanning TEM (HAADF-STEM) (Fig.S1) and extra EDS analysis individually against core or shell part of the Au@CdSe core-shell nanorods (Fig. S2). These results confirmed that Au is present at the core while Cd and Se are localize at the shell.

During synthesis, we can precisely control the shell thickness of Au@CdSe core@shell heterostructures by addition of different amounts of aqueous $Cd(NO_3)_2$. Fig. 5 shows TEM images of Au@CdSe hybrid structures with various shell thicknesses ranging from 1.7 nm to 8 nm. The table in Fig. 5 shows the dimensions of Au@CdSe hybrid structures. Fig. 6 shows the influence of fine tuning the thickness of the CdSe shell on the optical properties. When the shell thickness is increased, a redshift of both the LSPR and TSPR bands can be observed. This result arises from the higher effective refractive index around the Au nanorods with increasing shell thickness. We also calculated LSPR wavelength of Au@CdSe nanorods as a function of shell thickness using Gans theory[6]. (see supporting

information and Fig. S3) The core dimension was fixed as 10 × 30 nm while the shell thickness varied at the range of 1.7 ~ 8 nm. We observed a red-shift of SPR peak with increasing shell thickness consistent with our experimental results.

Single-particle DFS measurements suggest an efficient electron transfer from the Au nanorod to the CdSe shell in Au@CdSe nanorods when exciting the SPR. In order to obtain reasonable signal to noise ratios for DFS spectra of single Au@CdSe nanorods, we synthesized bare nanorods with dimension of 65 x 25 nm and grew a CdSe layer with thickness of 6 ~ 8 nm. The symbols in Fig. 7a and 7b represent the DFS spectra of single bare Au and Au@CdSe nanorods respectively with their corresponding SEM images shown as insets. The peak positions and the widths of the plasmon spectra were obtained by fitting the DFS spectra to a Lorentzian function (solid lines in Fig. 7 a, and b). For bare Au nanorods, the peak positions were 700 nm (upper) and 680 nm (lower), while those for the Au@CdSe nanorods were 728 nm (upper) and 736 nm (lower). The redshift of the plasmon band in Au@CdSe nanorods compared to the bare Au nanorods arises from the higher refractive index of the CdSe layer compared to the effective refractive index of air and the quartz substrate. More interestingly, the spectral linewidths of Au@CdSe nanorods were 80 nm (upper line in Fig. 7b) and 81 nm (lower line in Fig. 7b) in comparison to the bare Au nanorods with plasmon linewidths of 48 nm (upper line in Fig. 7a) and 44 nm (lower line in Fig. 7a). Additionally, the intensity of the plasmon band is ~ one order of magnitude higher in the bare Au nanorods compared to the Au@CdSe nanorods (Fig. S4). The broader linewidths and lower intensity in the scattering spectra of the Au@CdSe nanorods suggests chemical damping of the SPR arising from energy or more likely electron transfer from the Au to the CdSe layer, which is consistent with the results reported by Lian et al..[63] An increase in radiation damping can be ruled out because of the similar size of the bare Au

nanorods compared to that of the Au@CdSe nanorods as confirmed by SEM. Interband damping furthermore is smaller for the Au@CdSe nanorods because of the redshifted SPR.

After accomplishing the synthesis and characterization of the Au@CdSe hybrid structures, we further studied their application in photocatalysis under UV illumination. The effectiveness of metal@semiconductor heterostructures for photocatalysis depends on charge separation at the interface of the hybrid structures, which can overcome the obstacle of rapid electron-hole recombination in the semiconductor[46,47]. Due to their well-controlled composition and morphology, the Au@CdSe hybrid structures provide an ideal platform to investigate photocatalysis. In this work, the Au@CdSe hybrid nanorods were utilized to study the relationship between their photocatalytic properties and CdSe shell thickness. The photocatalytic activity of bare Au nanorods was also tested for comparison. MB was used as an electron acceptor and DI water produces abundant OH radicals which participate the degradation of MB molecules. The photocatalytic degradation of MB in aqueous solution under UV irradiation of bare Au nanorods and Au@CdSe hybrid structures is shown in Fig. 8a and 8b, respectively. The double peak feature of MB at 609 nm and 667 nm is clearly seen in the spectra. It should be noted that there is no MB photodegradation under UV irradiation in the absence of the CdSe component. These results demonstrate that the Au@CdSe hybrid structures exhibited much better photocatalytic efficiency than bare Au nanorods, which showed no loss of MB absorption under irradiation. The mechanism for MB photodegradation using the Au@CdSe hybrid structure as a photocatalyst can be described by the following steps[64]:

$$Au@CdSe + h\nu \rightarrow Au(e^-)@CdSe(h^+) \quad (1)$$

$$Au(e^-)@CdSe(h^+) + H_2O \rightarrow Au(e^-)@CdSe + H^+ + OH^\bullet \quad (2)$$

$MB + OH^{\bullet} \rightarrow$ degradation products (3)

Under UV light irradiation, charge separation took place within the Au@CdSe hybrid structures, resulting in electron transfer to the Au core and residual holes in the CdSe shell (eq. 1). Next, the light-induced holes transferred to the surface of the heterostructures and reacted with DI water to produce hydroxyl radicals (eq. 2). The MB molecule was decomposed by hydroxyl radicals and formed colorless leucomethylene blue (MBH) (eq. 3). Once the light-induced holes were exhausted in the photocatalytic reaction, Au@CdSe heterostructures reached an equilibrium Fermi level because of the accumulation of the photoexcited electrons[65]. The enhanced photocatalytic efficiency may be a consequence of the charge-transfer kinetics in the synergetic Au@CdSe hybrid structures.

The photocatalytic performance of Au@CdSe hybrid structures with different shell thicknesses were further compared in Fig. 9. For Au@CdSe hybrid structures with a shell thickness range of 2~3 nm, over 60% of MB was degraded within 30 minutes under UV light irradiation. A thicker shell in the range of 6~8 nm showed poor photodegradation of MB with the same exposure time, and structures with a shell thickness in the range of 9~11 nm showed even lower activity. From the above observations, we conclude that the photocatalytic activity of the Au@CdSe hybrid structures decreased with increasing shell thickness. This relationship may originate from the shorter diffusion distance of holes to the shell/solution interface, where the catalytic reactions occur, with thinner shell thickness. A shorter diffusion distance reduces the probability of electron-hole recombination at the Au/CdSe interface. It is noted that the fully covered shell of the Au@CdSe nanorods might trap carriers on the metal core, which leads to the degradation of the lifetime of a catalyst. This disadvantage can be overcome by a new designed

of Au@CdSe nanorods where the end of the Au nanorods was not covered by CdSe as shown in Fig. S1.

4. Conclusions

To summarize, we have developed a facile approach for the synthesis of Au@CdSe nanorods with complete core-shell structures. This strategy employs pre-growth of Ag_2Se as an intermediate layer that favors the formation of the CdSe shell by a cation-exchange process. Due to the large lattice mismatch of bulk Au and CdSe, Au@CdSe represents a model system to illustrate the mechanism for the synthesis of metal@semiconductor core-shell heteroepitaxial nanorods. Furthermore, the obtained Au@CdSe nanorods demonstrated that the shell thickness influenced the SPR. Moreover, light-induced charge separation was demonstrated in the Au@CdSe hybrid structures, and the highest photocatalytic efficiency was achieved with the thinnest CdSe shell. Looking forward, the as-obtained heterostructures with tunable shell thicknesses are expected to provide alternative substrates for various applications such as solar cells and biological detection due to their unique morphology and optical properties

Acknowledgement

The authors acknowledge the financial support by the National Science Council of Taiwan (NSC 102-2221-E-007-023-MY3, NSC 102-2221-E-007 -090 -MY2, and NSC 101-2623-E-007) , S.L. acknowledges the support from the Robert A. Welch Foundation (C-1664) and the Air Force Office of Scientific Research (MURI FA9550-15-1-0022). A.R.J. acknowledges support from the National Science Foundation Graduate Research Fellowship Program under Grant No. (1450681).

References

[1] K. Awazu, M. Fujimaki, C. Rockstuhl, J. Tominaga, H. Murakami, Y. Ohki, N. Yoshida, T. Watanabe, A plasmonic photocatalyst consisting of sliver nanoparticles embedded in titanium dioxide, J. Am. Chem. Soc. 130(5) (2008) 1676-1680.

[2] J.T. Li, S.K. Cushing, J. Bright, F.K. Meng, T.R. Senty, P. Zheng, A.D. Bristow, N.Q. Wu, Ag@Cu_2O Core-Shell Nanoparticles as Visible-Light Plasmonic Photocatalysts, Acs Catal. 3(1) (2013) 47-51.

[3] S.K. Cushing, J.T. Li, J. Bright, B.T. Yost, P. Zheng, A.D. Bristow, N.Q. Wu, Controlling Plasmon-Induced Resonance Energy Transfer and Hot Electron Injection Processes in Metal@TiO_2 Core-Shell Nanoparticles, J. Phys. Chem. C 119(28) (2015) 16239-16244.

[4] Y. Cao, T. Xie, R.C. Qian, Y.T. Long, Plasmon Resonance Energy Transfer: Coupling between Chromophore Molecules and Metallic Nanoparticles, Small 13(2) (2017).

[5] A.K. Samal, L. Polavarapu, S. Rodal-Cedeira, L.M. Liz-Marzan, J. Perez-Juste, I. Pastoriza-Santos, Size Tunable Au@Ag Core Shell Nanoparticles: Synthesis and Surface-Enhanced Raman Scattering Properties, Langmuir 29(48) (2013) 15076-15082.

[6] M.Z. Liu, P. Guyot-Sionnest, Synthesis and optical characterization of Au/Ag core/shell nanorods, J. Phys. Chem. B 108(19) (2004) 5882-5888.

[7] J. Yun, S.H. Hwang, J. Jang, Fabrication of Au@Ag Core/Shell Nanoparticles Decorated TiO_2 Hollow Structure for Efficient Light-Harvesting in Dye-Sensitized Solar Cells, Acs Appl. Mater. Inter. 7(3) (2015) 2055-2063.

[8] W.L. Shi, H. Zeng, Y. Sahoo, T.Y. Ohulchanskyy, Y. Ding, Z.L. Wang, M. Swihart, P.N. Prasad, A general approach to binary and ternary hybrid nanocrystals, Nano Lett. 6(4) (2006) 875-881.

[9] H. Yu, M. Chen, P.M. Rice, S.X. Wang, R.L. White, S.H. Sun, Dumbbell-like bifunctional Au-Fe_3O_4 nanoparticles, Nano Lett. 5(2) (2005) 379-382.

[10] S. Liu, S.J. Guo, S. Sun, X.Z. You, Dumbbell-like Au-Fe_3O_4 nanoparticles: a new nanostructure for supercapacitors, Nanoscale 7(11) (2015) 4890-4893.

[11] X.W. Meng, B. Li, X.L. Ren, L.F. Tan, Z.B. Huang, F.Q. Tang, One-pot gradient solvothermal synthesis of Au-Fe_3O_4 hybrid nanoparticles for magnetically recyclable catalytic applications, J. Mater. Chem. A 1(35) (2013) 10513-10517.

[12] L. Zhang, D.A. Blom, H. Wang, Au-Cu_2O Core-Shell Nanoparticles: A Hybrid Metal-Semiconductor Heteronanostructure with Geometrically Tunable Optical Properties, Chem. Mater. 23(20) (2011) 4587-4598.

[13] J.S. Lee, E.V. Shevchenko, D.V. Talapin, Au-PbS core-shell nanocrystals: Plasmonic absorption enhancement and electrical doping via intra-particle charge transfer, J. Am. Chem. Soc. 130(30) (2008) 9673-9674.

[14] S.K. Dutta, S.K. Mehetor, N. Pradhan, Metal Semiconductor Heterostructures for Photocatalytic Conversion of Light Energy, J. Phys. Chem. Lett. 6(6) (2015) 936-944.

[15] B.K. Patra, S. Khilari, D. Pradhan, N. Pradhan, Hybrid Dot-Disk Au-$CuInS_2$ Nanostructures as Active Photocathode for Efficient Evolution of Hydrogen from Water, Chem. Mater. 28(12) (2016) 4358-4366.

[16] Y.W. Cao, U. Banin, Growth and properties of semiconductor core/shell nanocrystals with InAs cores, J. Am. Chem. Soc. 122(40) (2000) 9692-9702.

[17] W. van der Stam, E. Bladt, F.T. Rabouw, S. Bals, C.D. Donega, Near-Infrared Emitting $CuInSe_2$/$CuInS_2$ Dot Core/Rod Shell Heteronanorods by Sequential Cation Exchange, Acs Nano 9(11) (2015) 11430-11438.

[18] X.F. Wu, H.Y. Song, J.M. Yoon, Y.T. Yu, Y.F. Chen, Synthesis of Core-Shell Au@TiO_2 Nanoparticles with Truncated Wedge-Shaped Morphology and Their Photocatalytic Properties, Langmuir 25(11) (2009) 6438-6447.

[19] N. Zhang, S.Q. Liu, X.Z. Fu, Y.J. Xu, Synthesis of M@TiO_2 (M = Au, Pd, Pt) Core-Shell Nanoconnposites with Tunable Photoreactivity, J. Phys. Chem. C 115(18) (2011) 9136-9145.

[20] D.J. Zheng, X.C. Pang, M.Y. Wang, Y.J. He, C.J. Lin, Z.Q. Lin, Unconventional Route to Hairy Plasmonic/Semiconductor Core/Shell Nanoparticles with Precisely Controlled Dimensions and Their Use in Solar Energy Conversion, Chem. Mater. 27(15) (2015) 5271-5278.

[21] W.T. Chen, T.T. Yang, Y.J. Hsu, Au-CdS Core-Shell Nanocrystals with Controllable Shell Thickness and Photoinduced Charge Separation Property, Chem. Mater. 20(23) (2008) 7204-7206.

[22] Y. Kobayashi, Y. Nonoguchi, L. Wang, T. Kawai, N. Tamai, Dual Transient Bleaching of Au/PbS Hybrid Core/Shell Nanoparticles, J. Phys. Chem. Lett. 3(9) (2012) 1111-1116.

[23] Z.X. Fan, X. Zhang, J. Yang, X.J. Wu, Z.D. Liu, W. Huang, H. Zhang, Synthesis of 4H/fcc-Au@Metal Sulfide Core Shell Nanoribbons, J. Am. Chem. Soc. 137(34) (2015) 10910-10913.

[24] E. Elmalem, A.E. Saunders, R. Costi, A. Salant, U. Banin, Growth of Photocatalytic CdSe-Pt Nanorods and Nanonets, Adv. Mater. 20(22) (2008) 4312-4317.

[25] D. Li, Y.N. Xia, Fabrication of titania nanofibers by electrospinning, Nano Lett. 3(4) (2003) 555-560.

[26] Z.H. Sun, Z. Yang, J.H. Zhou, M.H. Yeung, W.H. Ni, H.K. Wu, J.F. Wang, A General Approach to the Synthesis of Gold-Metal Sulfide Core-Shell and Heterostructures, Angew. Chem. Int. Ed. 48(16) (2009) 2881-2885.

[27] V. Subramanian, E.E. Wolf, P.V. Kamat, Influence of metal/metal ion concentration on the photocatalytic activity of TiO_2-Au composite nanoparticles, Langmuir 19(2) (2003) 469-474.

[28] Y. Tian, T. Tatsuma, Mechanisms and applications of plasmon-induced charge separation at TiO_2 films loaded with gold nanoparticles, J. Am. Chem. Soc. 127(20) (2005) 7632-7637.

[29] R. Marschall, Semiconductor Composites: Strategies for Enhancing Charge Carrier Separation to Improve Photocatalytic Activity, Adv. Funct. Mater. 24(17) (2014) 2421-2440.

[30] K. Okamoto, I. Niki, A. Shvartser, Y. Narukawa, T. Mukai, A. Scherer, Surface-plasmon-enhanced light emitters based on InGaN quantum wells, Nat. Mater. 3(9) (2004) 601-605.

[31] T. Mokari, E. Rothenberg, I. Popov, R. Costi, U. Banin, Selective growth of metal tips onto semiconductor quantum rods and tetrapods, Science 304(5678) (2004) 1787-1790.

[32] N. Zhang, S.Q. Liu, Y.J. Xu, Recent progress on metal core@semiconductor shell nanocomposites as a promising type of photocatalyst, Nanoscale 4(7) (2012) 2227-2238.

[33] H.J. Wang, K.H. Yang, S.C. Hsu, M.H. Huang, Photothermal effects from Au-Cu_2O core-shell nanocubes, octahedra, and nanobars with broad near-infrared absorption tunability, Nanoscale 8(2) (2016) 965-972.

[34] S. Rej, H.J. Wang, M.X. Huang, S.C. Hsu, C.S. Tan, F.C. Lin, J.S. Huang, M.H. Huang, Facet-dependent optical properties of Pd-Cu_2O core-shell nanocubes and octahedra, Nanoscale 7(25) (2015) 11135-11141.

[35] S.E. Habas, P.D. Yang, T. Mokari, Selective growth of metal and binary metal tips on CdS nanorods, J. Am. Chem. Soc. 130(11) (2008) 3294-3295.

[36] G. Menagen, J.E. Macdonald, Y. Shemesh, I. Popov, U. Banin, Au Growth on Semiconductor Nanorods: Photoinduced versus Thermal Growth Mechanisms, J. Am. Chem. Soc. 131(47) (2009) 17406-17411.

[37] R. Costi, A.E. Saunders, E. Elmalem, A. Salant, U. Banin, Visible light-induced charge retention and photocatalysis with hybrid CdSe-Au nanodumbbells, Nano Lett. 8(2) (2008) 637-641.

[38] U. Banin, Y. Ben-Shahar, K. Vinokurov, Hybrid Semiconductor-Metal Nanoparticles: From Architecture to Function, Chem. Mater. 26(1) (2014) 97-110.

[39] Y. Nakibli, L. Amirav, Selective Growth of Ni Tips on Nanorod Photocatalysts, Chem. Mater. 28(13) (2016) 4524-4527.

[40] F.R. Fan, Y. Ding, D.Y. Liu, Z.Q. Tian, Z.L. Wang, Facet-Selective Epitaxial Growth of Heterogeneous Nanostructures of Semiconductor and Metal: ZnO Nanorods on Ag Nanocrystals, J. Am. Chem. Soc. 131(34) (2009) 12036-12037.

[41] V. Fernandez-Altable, M. Dalmases, A. Falqui, A. Casu, P. Torruella, S. Estrade, F. Peiro, A. Figuerola, Au-Assisted Growth of Anisotropic and Epitaxial CdSe Colloidal Nanocrystals via in Situ Dismantling of Quantum Dots, Chem. Mater. 27(5) (2015) 1656-1664.

[42] Y.Z. Chen, D.Q. Zeng, M.B. Cortie, A. Dowd, H.Z. Guo, J.B. Wang, D.L. Peng, Seed-Induced Growth of Flower-Like Au-Ni-ZnO Metal-Semiconductor Hybrid Nanocrystals for Photocatalytic Applications, Small 11(12) (2015) 1460-1469.

[43] D.H. Son, S.M. Hughes, Y.D. Yin, A.P. Alivisatos, Cation exchange reactions-in ionic nanocrystals, Science 306(5698) (2004) 1009-1012.

[44] R.D. Robinson, B. Sadtler, D.O. Demchenko, C.K. Erdonmez, L.W. Wang, A.P. Alivisatos, Spontaneous superlattice formation in nanorods through partial cation exchange, Science 317(5836) (2007) 355-358.

[45] B. Sadtler, D.O. Demchenko, H. Zheng, S.M. Hughes, M.G. Merkle, U. Dahmen, L.W. Wang, A.P. Alivisatos, Selective Facet Reactivity during Cation Exchange in Cadmium Sulfide Nanorods, J. Am. Chem. Soc. 131(14) (2009) 5285-5293.

[46] U.Y. Jeong, P.H.C. Camargo, Y.H. Lee, Y.N. Xia, Chemical transformation: a powerful route to metal chalcogenide nanowires, J. Mater. Chem. 16(40) (2006) 3893-3897.

[47] G.D. Moon, S. Ko, Y. Min, J. Zeng, Y.N. Xia, U. Jeong, Chemical transformations of nanostructured materials, Nano Today 6(2) (2011) 186-203.

[48] A. Dawson, P.V. Kamat, Semiconductor-metal nanocomposites. Photoinduced fusion and photocatalysis of gold-capped TiO_2 (TiO_2/Gold) nanoparticles, J. Phys. Chem. B 105(5) (2001) 960-966.

[49] H.X. Li, Z.F. Bian, J. Zhu, Y.N. Huo, H. Li, Y.F. Lu, Mesoporous Au/TiO_2 nanocomposites with enhanced photocatalytic activity, J. Am. Chem. Soc. 129(15) (2007) 4538-4539.

[50] P. Li, Z. Wei, T. Wu, Q. Peng, Y.D. Li, Au-ZnO Hybrid Nanopyramids and Their Photocatalytic Properties, J. Am. Chem. Soc. 133(15) (2011) 5660-5663.

[51] T. Hirakawa, P.V. Kamat, Charge separation and catalytic activity of Ag@TiO_2 core-shell composite clusters under UV-irradiation, J. Am. Chem. Soc. 127(11) (2005) 3928-3934.

[52] T.T. Yang, W.T. Chen, Y.J. Hsu, K.H. Wei, T.Y. Lin, T.W. Lin, Interfacial Charge Carrier Dynamics in Core-Shell Au-CdS Nanocrystals, J. Phys. Chem. C 114(26) (2010) 11414-11420.

[53] Y.Z. Chen, D.Q. Zeng, K. Zhang, A.L. Lu, L.S. Wang, D.L. Peng, Au-ZnO hybrid nanoflowers, nanomultipods and nanopyramids: one-pot reaction synthesis and photocatalytic properties, Nanoscale 6(2) (2014) 874-881.

[54] X. Yang, H. Li, W. Zhang, M.X. Sun, L.Q. Li, N. Xu, J.D. Wu, J. Sun, High Visible Photoelectrochemical Activity of Ag Nanoparticle-Sandwiched CdS/Ag/ZnO Nanorods, Acs Appl. Mater. Inter. 9(1) (2017) 658-667.

[55] P.V. Kamat, M. Flumiani, A. Dawson, Metal-metal and metal-semiconductor composite nanoclusters, Colloid Surface A 202(2-3) (2002) 269-279.

[56] M. Sykora, M.A. Petruska, J. Alstrum-Acevedo, I. Bezel, T.J. Meyer, V.I. Klimov, Photoinduced charge transfer between CdSe nanocrystal quantum dots and Ru-polypyridine complexes, J. Am. Chem. Soc. 128(31) (2006) 9984-9985.

[57] P. Wang, A. Abrusci, H.M.P. Wong, M. Svensson, M.R. Andersson, N.C. Greenham, Photoinduced charge transfer and efficient solar energy conversion in a blend of a red polyfluorene copolymer with CdSe nanoparticles, Nano Lett. 6(8) (2006) 1789-1793.

[58] W.U. Huynh, J.J. Dittmer, A.P. Alivisatos, Hybrid nanorod-polymer solar cells, Science 295(5564) (2002) 2425-2427.

[59] L.Z. Zhu, B.J. Richardson, Q.M. Yu, Inverted hybrid CdSe-polymer solar cells adopting PEDOT:PSS/MoO_3 as dual hole transport layers, Phys. Chem. Chem. Phys. 18(5) (2016) 3463-3471.

[60] S. Khanchandani, S. Kundu, A. Patra, A.K. Ganguli, Shell Thickness Dependent Photocatalytic Properties of ZnO/CdS Core-Shell Nanorods, J. Phys. Chem. C 116(44) (2012) 23653-23662.

[61] L. Dloczik, R. Konenkamp, Nanostructure transfer in semiconductors by ion exchange, Nano Lett. 3(5) (2003) 651-653.

[62] M.Z. Liu, P. Guyot-Sionnest, Preparation and optical properties of silver chalcogenide coated gold nanorods, J. Mater. Chem. 16(40) (2006) 3942-3945.

[63] K. Wu, J. Chen, J.R. McBride, T. Lian, Efficient hot-electron transfer by a plasmon-induced interfacial charge-transfer transition, Science 349(6248) (2015) 632-635.

[64] A. Houas, H. Lachheb, M. Ksibi, E. Elaloui, C. Guillard, J.M. Herrmann, Photocatalytic degradation pathway of methylene blue in water, Appl. Catal. B-Environ. 31(2) (2001) 145-157.

[65] M. Jakob, H. Levanon, P.V. Kamat, Charge distribution between UV-irradiated TiO_2 and gold nanoparticles: Determination of shift in the Fermi level, Nano Lett. 3(3) (2003) 353-358.

Figures

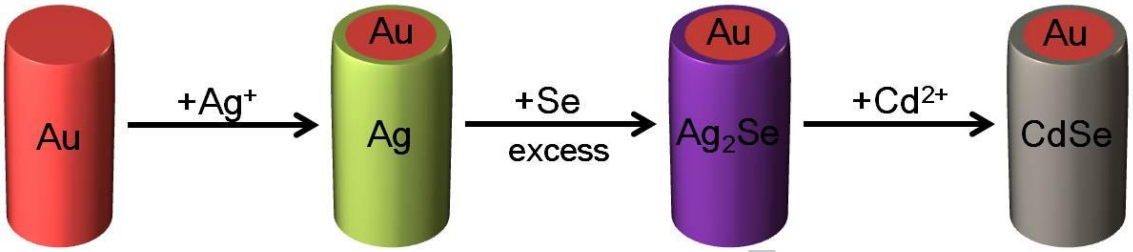

Scheme 1. Growth scheme of Au@CdSe core-shell nanorods.

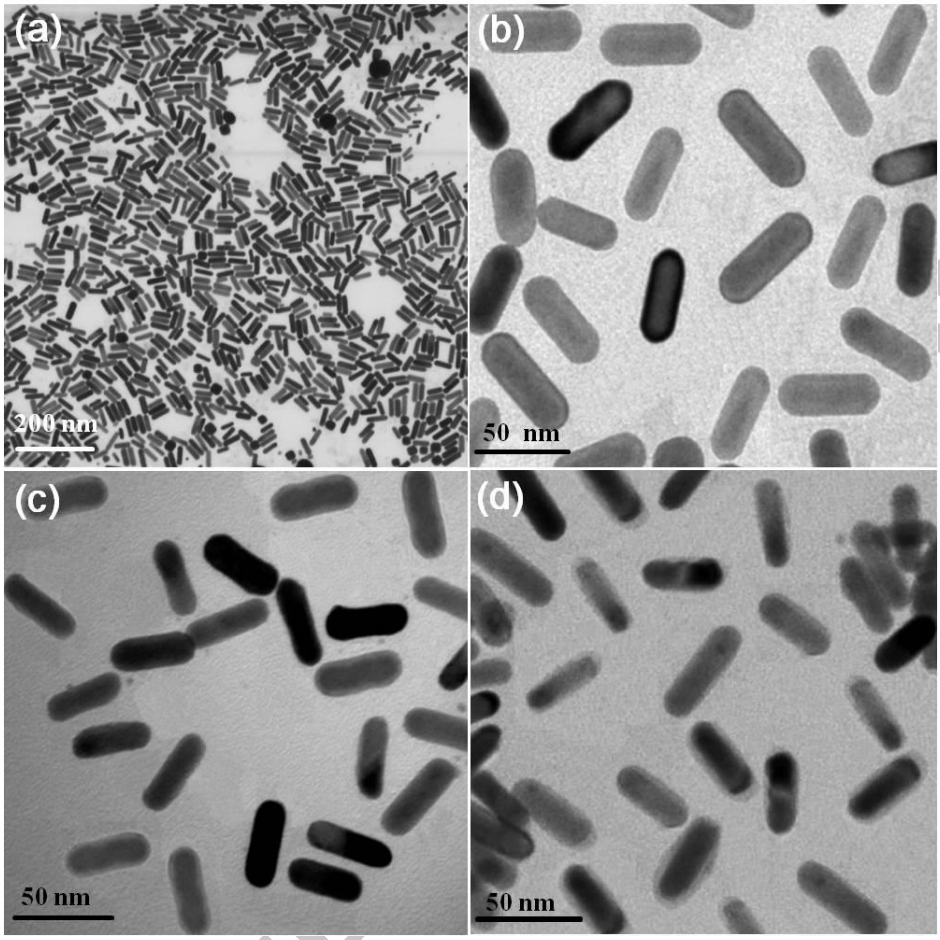

Fig. 1. TEM images of (a) original bare Au nanorods, (b) Au@Ag, (c) Au@Ag_2Se core-shell nanorods, (d) Au@CdSe core-shell nanorods with a shell thickness of 3.6 nm.

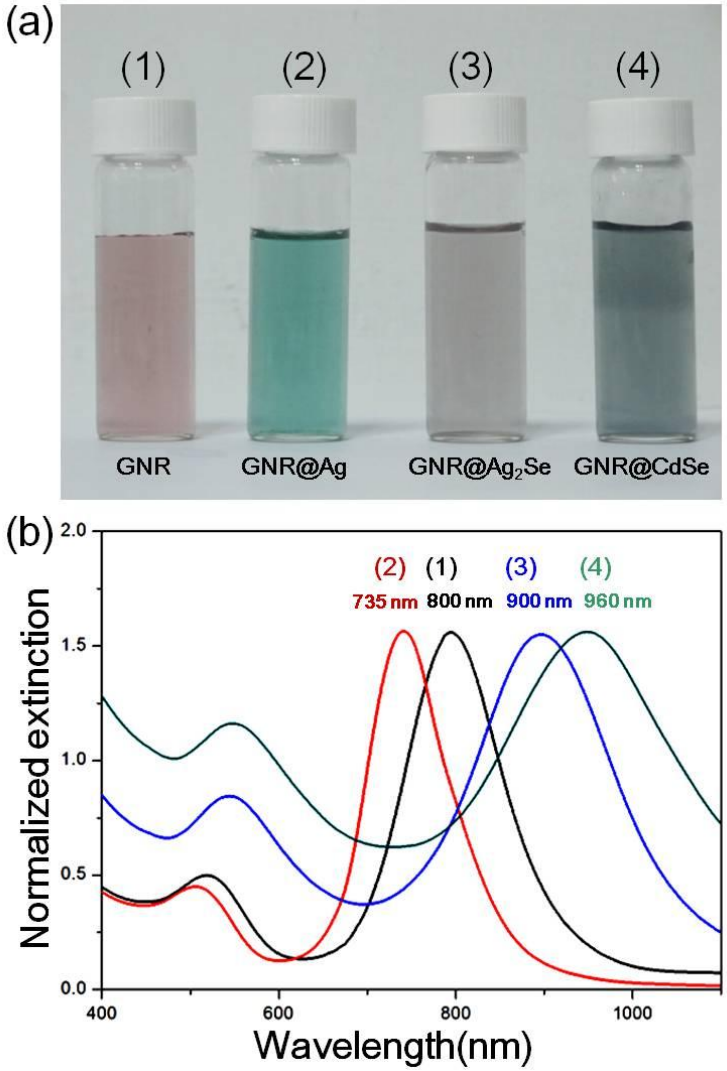

Fig. 2. (a) Photo and (b) normalized absorption spectra of (1) bare Au, (2) Au@Ag, (3) Au@Ag_2Se and (4) Au@CdSe core-shell nanorods.

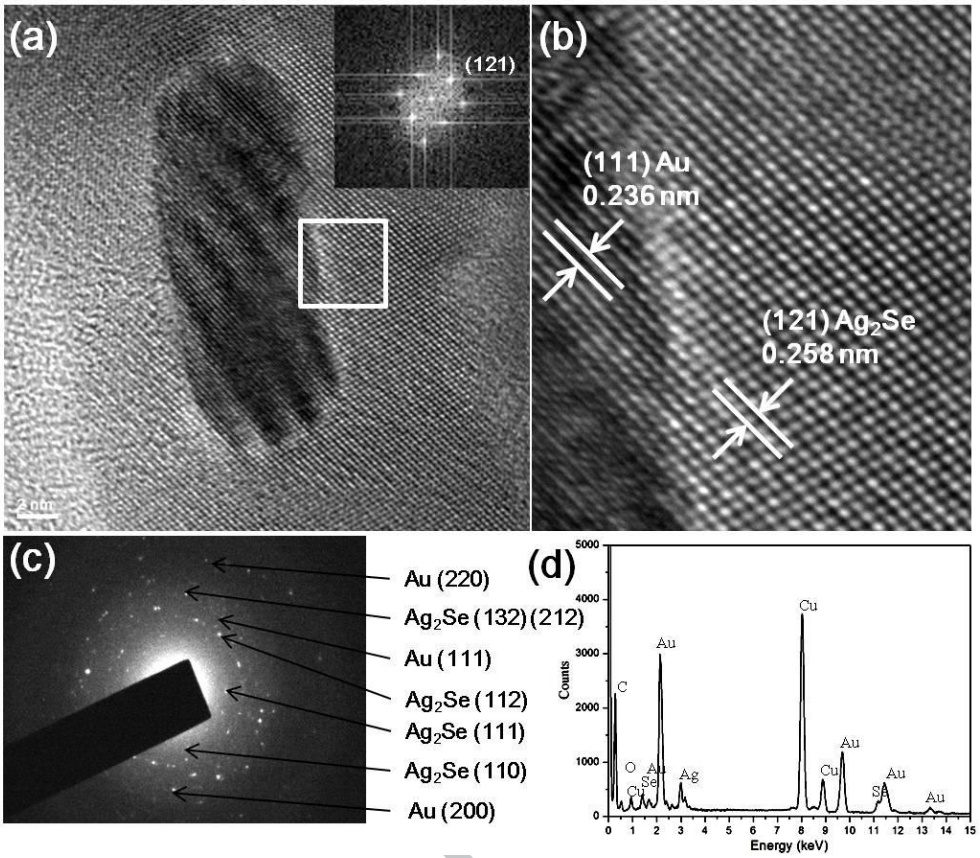

Fig. 3. (a-b) HRTEM image (c) SAED pattern (d) EDS analysis spectrum of Au@Ag_2Se core-shell nanorods. The inset in (a) shows the FFT pattern of the selected square region in the image, illustrating the (121) crystal plane of the shell.

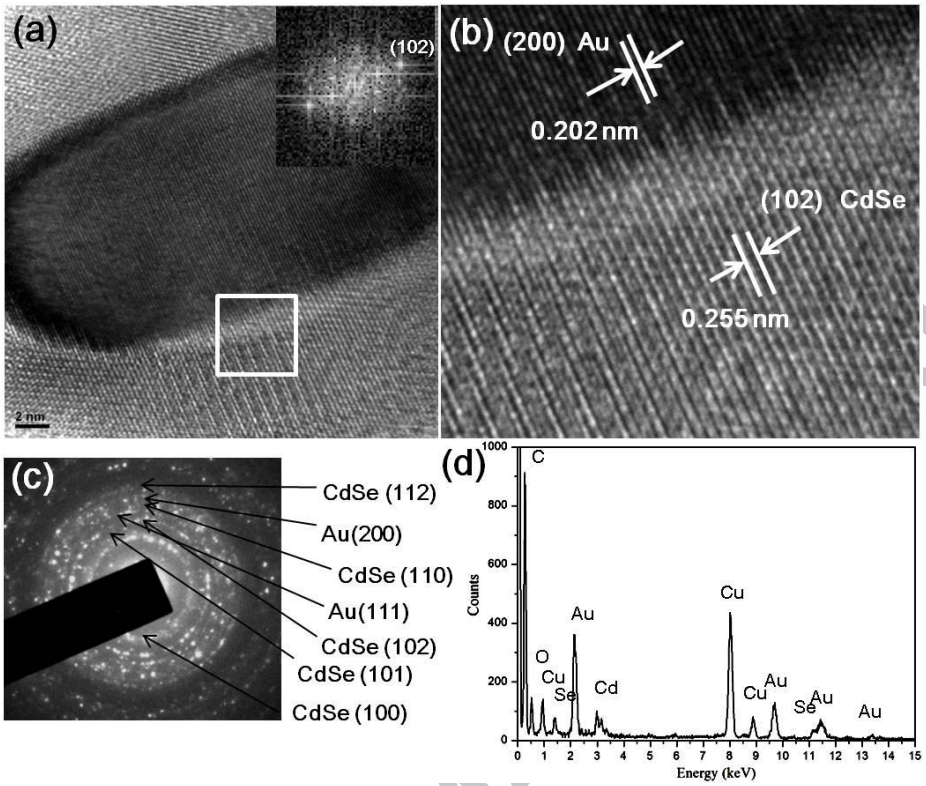

Fig. 4. (a-b) HRTEM image (c) SAED pattern (d) EDS analysis spectrum of Au@CdSe core-shell nanorods. The inset in (a) shows the FFT pattern of the selected square region in the image, illustrating the (102) crystal plane of the shell.

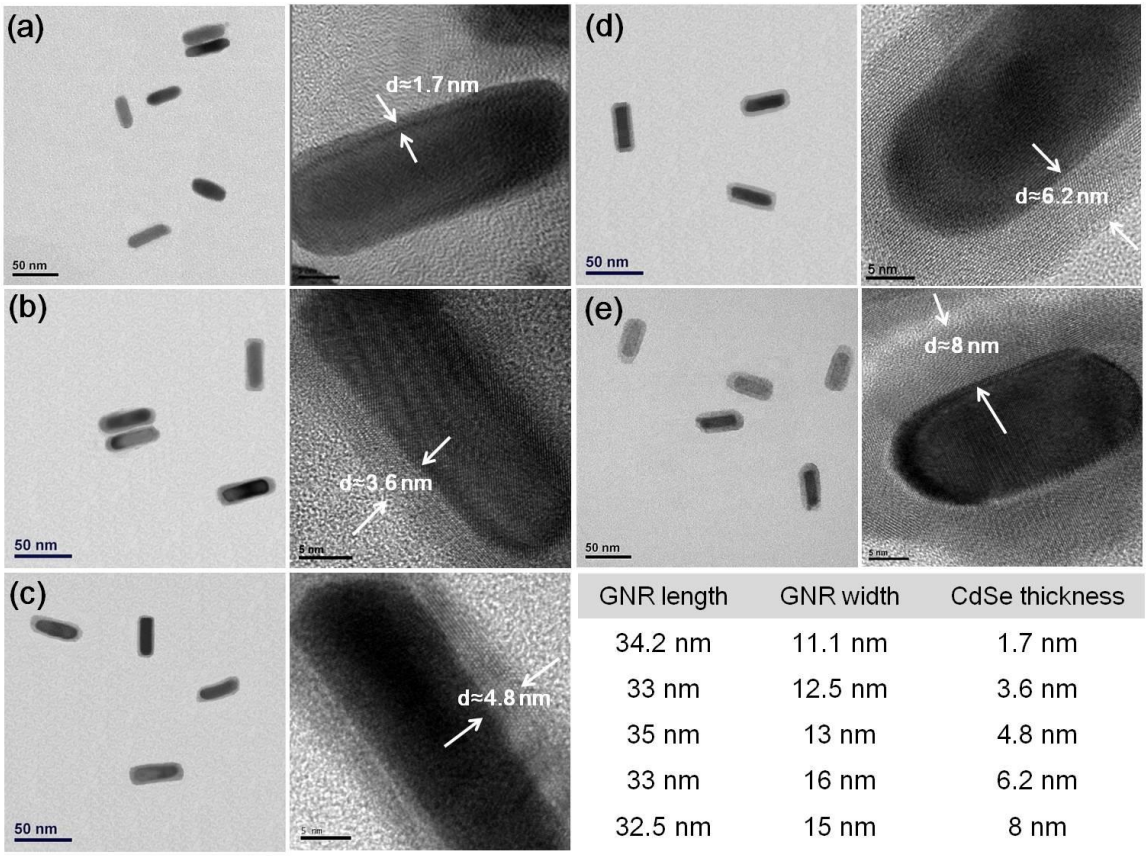

GNR length	GNR width	CdSe thickness
34.2 nm	11.1 nm	1.7 nm
33 nm	12.5 nm	3.6 nm
35 nm	13 nm	4.8 nm
33 nm	16 nm	6.2 nm
32.5 nm	15 nm	8 nm

Fig. 5. TEM images of Au@CdSe core-shell nanorods with CdSe shell thickness of (a) 1.7 nm, (b) 3.6 nm, (c) 4.8 nm, (d) 6.2 nm and (e) 8 nm. The insert is a table of Au@CdSe hybrid structures with dimensions and shell thickness

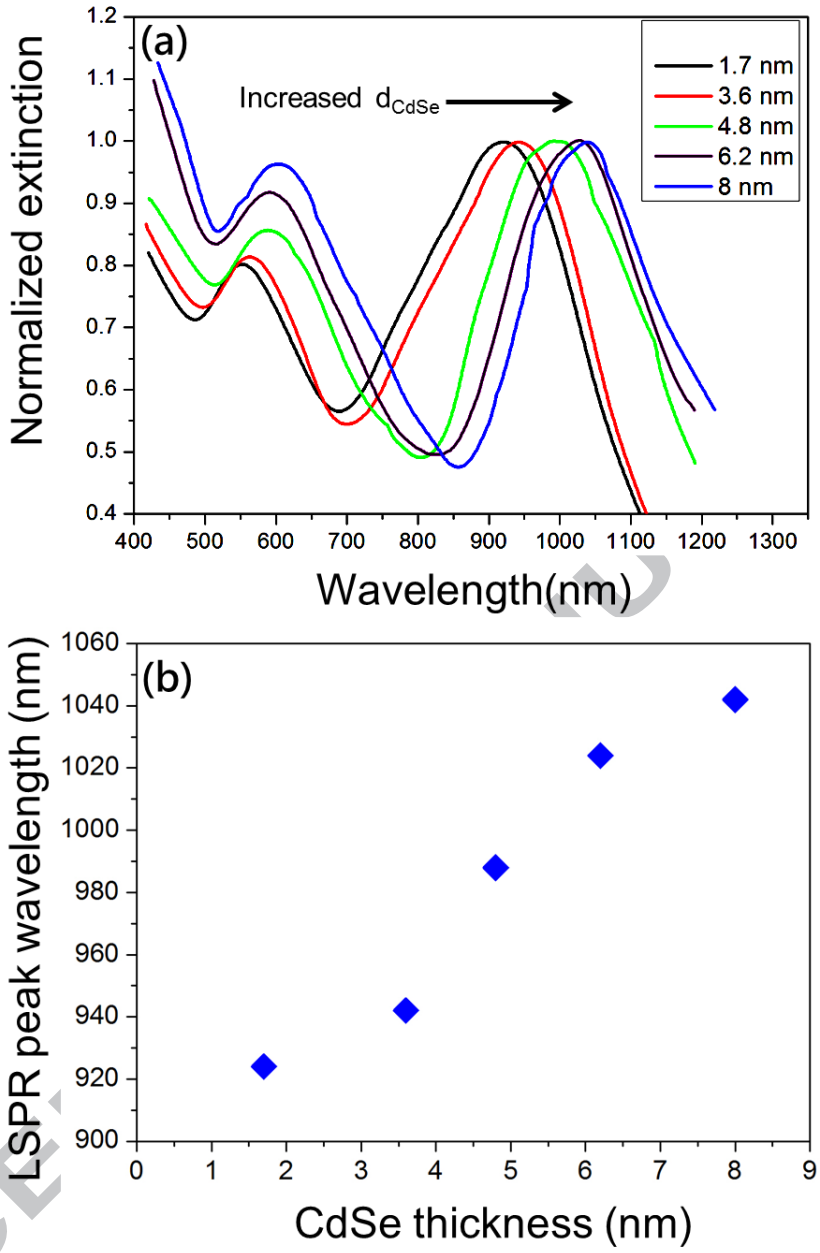

Fig. 6. (a) Normalized extinction spectrum of Au@CdSe core-shell structures with increased CdSe shell thickness *d*. (b) The relationship between LSPR peak wavelength and CdSe shell thickness.

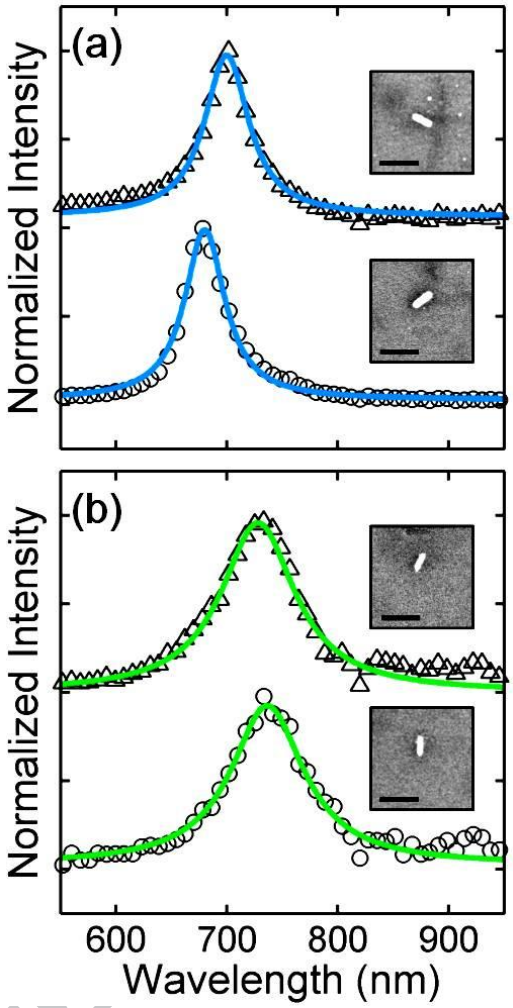

Fig. 7. Dark-field scattering spectra of single nanorods. (a) Bare Au nanorod scattering spectra (blue) with peak positions equal to 700 nm (upper) and 680 nm (lower), and linewidths of 48 nm (upper) and 44 nm (lower). Inset: the SEM images of measured bare Au nanorods with dimensions of 58 x 22 nm (upper) and 63 x 25 nm (lower) (b) Au@CdSe nanorod spectra (green) centered at 728 nm (upper) and 736 nm (lower) with linewidths of 80 nm (upper) and 81 nm (lower). Inset: SEM images of measured Au@CdSe nanorods with dimensions of 52 x 20 nm (upper) and 54 x 20 nm (lower). The scale bars of all SEM images indicate 100 nm. Peak positions and the homogenous linewidths were obtained by fitting the scattering spectra to a Lorentzian function (solid line).

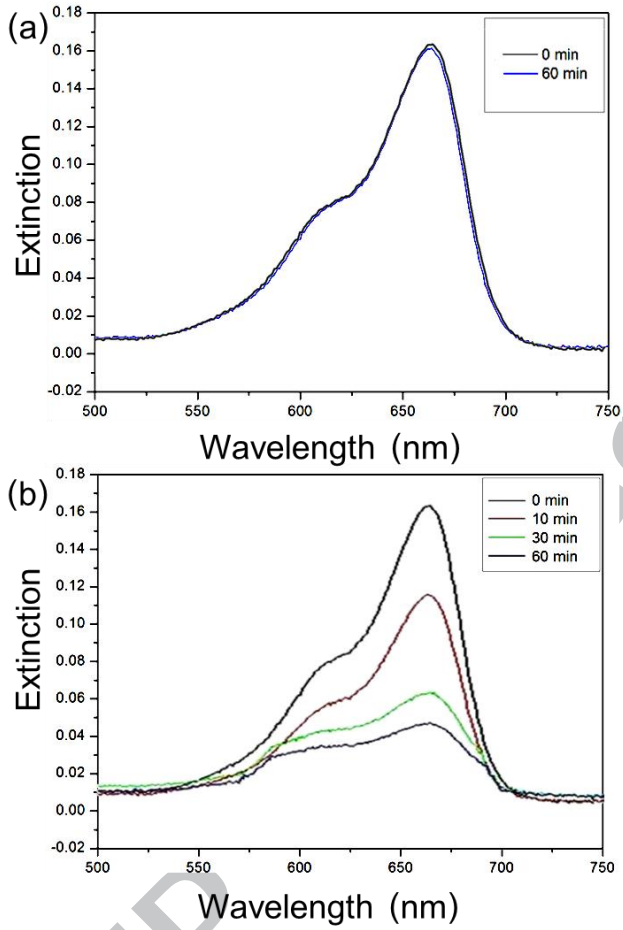

Fig. 8. Photodegradation of methylene blue dye molecules with (a) bare Au nanorods and (b) Au@CdSe nanorods core-shell nanorods photocatalysts with 4-5 nm shell thicknesses under UV irradiation for the same exposure times.

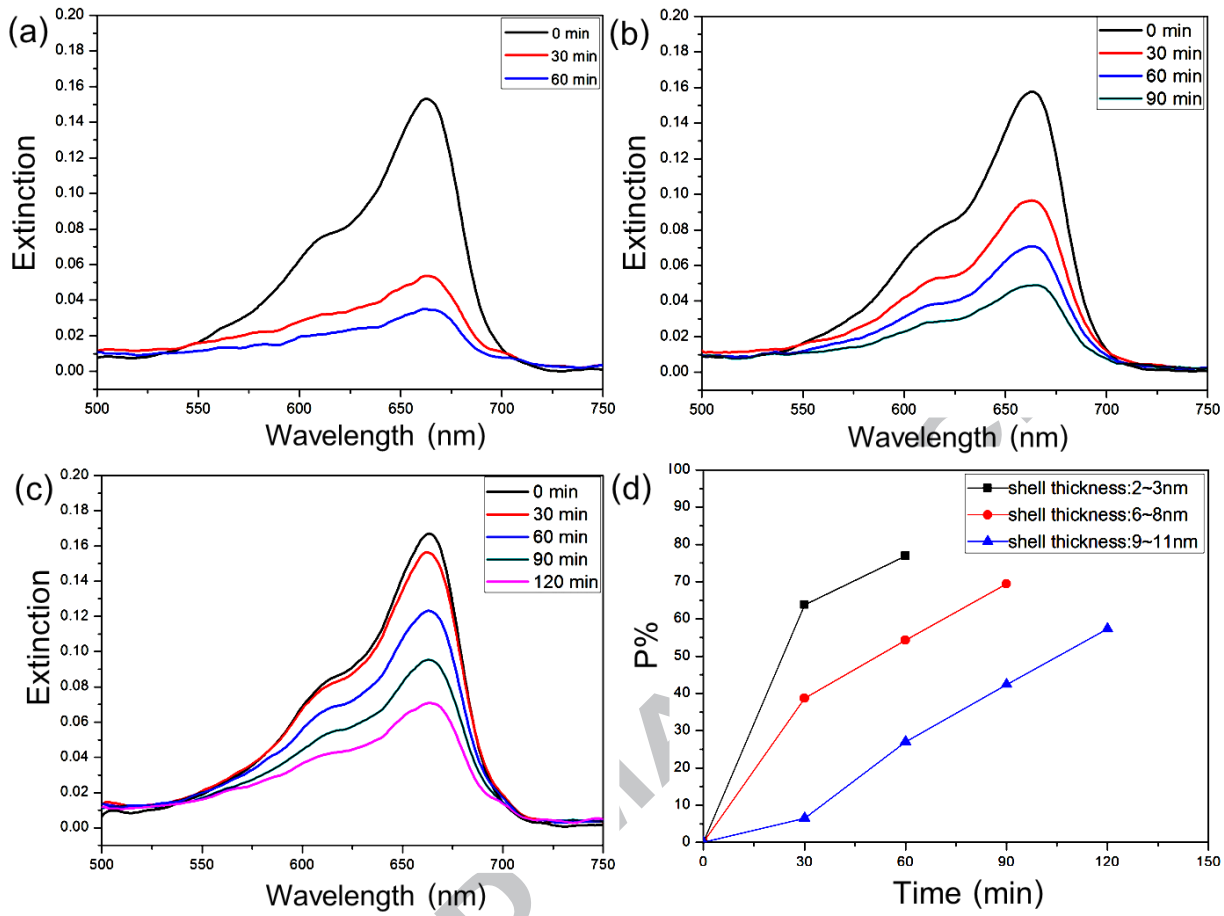

Fig. 9. Photocatalytic activity of the Au@CdSe core-shell nanorods. Degradation of MB by the Au@CdSe core-shell nanorods photocatalysts with different shell thicknesses: (a) 2~3 nm, (b) 6~8 nm and (c) 9~11 nm. (d) Photocatalytic efficiency comparison of Au@CdSe core-shell nanorods with different shell thicknesses.

Graphical abstract

Novel Au@CdSe heteroepitaxial nanorods were prepared via pre-growth of Ag_2Se as an intermediate layer that favored the formation of a complete CdSe shell via a cation-exchange process. The as-obtained heterostructures with tunable shell thicknesses are expected to provide alternative substrates for various applications such as solar cells and biological detection.